D. Invernizzi, M. Lovera
Trajectory Tracking Control of Thrust-Vectoring UAVs
Automatica, Vol. 95, 2018, p. 180-186
doi:10.1016/j.automatica.2018.05.024

Trajectory tracking control of thrust-vectoring UAVs

Davide Invernizzi [a], Marco Lovera [a]

[a] *Politecnico di Milano, Department of Aerospace Science and Technology, Via La Masa 34, 20156, Milano*

Abstract

In this paper a geometric approach to the trajectory tracking control of Unmanned Aerial Vehicles (UAVs) with thrust vectoring capabilities is proposed. The control problem is developed within the framework of geometric control theory, yielding a control law that is independent of any parametrization of the configuration space. The proposed design works seamlessly when the thrust vectoring capability is limited, by prioritizing position over attitude tracking. The control law guarantees almost-global asymptotic tracking of a desired full-pose (attitude and position) trajectory that is compatible with the platform underactuation according to a specific trackability condition. Finally, a numerical example is presented to test the proposed control law on a tilt-rotor quadcopter UAV. The generality of the control strategy can be exploited for a broad class of UAVs with thrust vectoring capabilities.

Key words: UAVs, thrust vectoring; trajectory tracking; geometric control.

1 Introduction

The development of Unmanned Aerial Vehicles (UAVs) with thrust vectoring capabilities has grown significantly in recent years. These aerial vehicles are endowed with a propulsion system that can deliver both a net torque and a force with respect to the aircraft frame, which makes them end-effector-like devices. Among the different technological solutions, several multirotor configurations have shown great potentiality in terms of fast disturbance rejection and maneuverability [8,4,6,17,14]. Indeed, while the standard coplanar multirotor architecture [1,12,10] combines good performance and a simple mechanical design, it is inherently underactuated as the control force can be applied only in a fixed direction of the aircraft frame. On the contrary, thrust vectoring vehicles overcome this intrinsic maneuverability limitation and widen the operational range of the conventional system. Among the different architectures that have been developed, it is worth mentioning the fixed-tilted hexacopter [14] and the tilt-rotor quadcopter [17].

The trajectory tracking control problem for these aerial vehicles is challenging for two main reasons: the maneuver may involve large rotational motions and there may be limitations in the thrust vectoring capability, thus reducing the actual maneuverability. In particular, propulsion systems of thrust-vectoring UAVs cannot usually deliver thrust in any direction of the aircraft frame [14], which makes the platform underactuated. These issues have been addressed explicitly in [6], in which the control strategy is based on prioritizing position over attitude tracking to handle the actuation limitation. The resulting control law guarantees almost-global tracking (in the sense of [9]) but requires a sufficiently fast loop for the stabilization of the angular velocity. Following similar ideas, [5] tackled the tracking problem for a more general class of UAVs with laterally bounded input force. The approach presented therein includes an optimization step to handle the actuation limitation but it guarantees only local exponential convergence of the tracking errors. Thrust vectoring control techniques have also been exploited to solve the position tracking problem of ducted-fan vehicles [13,1,16].

In this work, the trajectory tracking problem for UAVs with thrust vectoring capabilities is solved directly in $\mathrm{SO}(3) \times \mathbb{R}^3$, with thrust and torque as inputs. We start by showing that tracking of a desired full-pose trajectory (position and attitude) is not feasible if the thrust can be produced only in a cone region around the vertical body axis of the vehicle. However, by relaxing attitude tracking requirements, position tracking can always be achieved. In particular, a reference attitude, different from the desired one, is computed by means of a dynamic controller such that it is always possible to deliver the control force required to guarantee position tracking. Then, the modified attitude trajectory is used as the actual reference for the attitude control subsystem. By

Email addresses: davide.invernizzi@polimi.it (Davide Invernizzi), marco.lovera@polimi.it (Marco Lovera).

exploiting a geometric PID controller, the modified attitude motion is tracked even in the presence of a constant disturbance torque. We prove that under a specific trackability condition, also the desired attitude motion can be exactly tracked almost globally. By means of established cascade arguments [15,12], we demonstrate that our solution ensures almost-global asymptotic tracking (AGAT), which is the strongest result one can obtain on $\mathrm{SO}(3) \times \mathbb{R}^3$ with continuous time-invariant control laws [9]. Furthermore, the proposed control law improves the transient performance, in terms of position overshoot, with respect to the most common solution in the literature, as it is shown in a numerical example.

Notations. For $A \in \mathbb{R}^{n\times n}$, the minimum and maximum eigenvalues are denoted as $\lambda_m(A)$ and $\lambda_M(A)$, respectively, and $\mathrm{skew}(A) := \frac{A-A^T}{2}$ is the skew-symmetric part of A. The *i-th* canonical base in $\mathbb{R}^n$ is $e_i := [0 \cdots 1 \cdots 0]^T$, while the identity element in $\mathbb{R}^{n\times n}$ is $I_n := [e_1 \cdots e_n]$. Given the vectors a, b we often denote $(a, b) := [a^T, b^T]^T$. Given a bounded function $f : \mathbb{R} \to \mathbb{R}^n$, we denote the positive constants f_m and f_M as lower and upper bounds of f, respectively, such that $f_m \leq \|f(t)\| \leq f_M \ \forall t \in \mathbb{R}$. The *hat* map $\hat{\cdot} : \mathbb{R}^3 \to \mathfrak{so}(3)$ is an isomorphism between $\mathbb{R}^3$ and $\mathfrak{so}(3)$, the space of third order skew-symmetric matrices, such that $\hat{\omega}y = \omega \times y$, $\forall y \in \mathbb{R}^3$, where $\times$ is the cross product. The corresponding inverse is the *vee* map $(\cdot)^\vee : \mathfrak{so}(3) \to \mathbb{R}^3$. We will often employ the modified trace function $\Psi_K(R) := \frac{1}{2}\mathrm{tr}(K(I_3 - R))$, where $K = K^T \in \mathbb{R}^{3\times3}$ is such that $\mathrm{tr}(K)I_3 - K \in \mathbb{R}^{3\times3}_{>0}$, to measure attitude errors in $\mathrm{SO}(3)$. The time derivative of Ψ_K along the flows of $\dot{R} = R\hat{\omega}$ is $\dot{\Psi}_K(R) = e_R^T\omega$, where $e_R := \frac{\mathrm{skew}(KR-R^TK)^\vee}{2}$ is the left-trivialized derivative of Ψ_K. When K has distinct positive eigenvalues, Ψ_K is an example of polar Morse function [9].

2 Mathematical modeling

The class of aerial vehicles considered in this work can be described as rigid bodies subjected to external actions and with an actuation mechanism that can produce torque in any direction and thrust in a spherical sector around the vertical axis of the body frame.

2.1 Dynamical model

The motion of a rigid body is described by the motion of a body-fixed frame $\mathcal{F}_B = (O_B, \{b_1, b_2, b_3\})$ with respect to an inertial reference frame $\mathcal{F}_I = (O_I, \{e_1, e_2, e_3\})$, as shown in Figure 1 (for the sake of simplicity, we assume that the inertial frame axes coincide with the canonical basis of $\mathbb{R}^3$). The configuration of a rigid body is uniquely and globally defined by $G := (R, x) \in \mathrm{SO}(3)\times\mathbb{R}^3 =: \mathcal{M}$, where $R := [b_1\, b_2\, b_3] \in \mathrm{SO}(3)$ is the rotation matrix describing the orientation of $\mathcal{F}_B$ with respect to $\mathcal{F}_I$ and

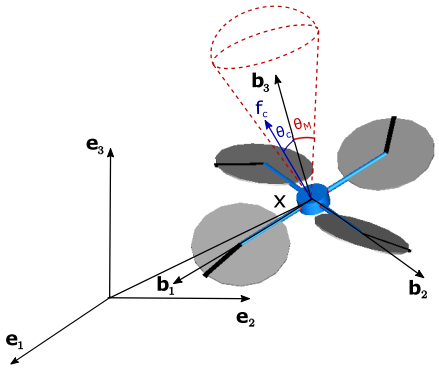

Fig. 1. Reference frames - tilt-rotor quadcopter UAV.

$x \in \mathbb{R}^3$ is the position vector of the origin O_B with respect to O_I, resolved in the reference frame $\mathcal{F}_I$. The tangent vector to a curve (velocity) at a given configuration $G \in \mathcal{M}$ is the pair $(\omega, v) \in T_R\mathrm{SO}(3) \times \mathbb{R}^3 \simeq T_G\mathcal{M}$, by direct identification of $\mathbb{R}^3$ with its tangent space $T_x\mathbb{R}^3$. The equations of motion of a rigid body moving in a constant gravity field $-ge_3$, actuated by a control wrench $(f_c, \tau_c) \in \mathbb{R}^3\times\mathbb{R}^3$ and subjected to external disturbances $(f_d, \tau_d) \in \mathbb{R}^3 \times \mathbb{R}^3$, which include unmodeled dynamics and aerodynamic effects, are described by the following system [12]:

$$\dot{x} = v \tag{1}$$
$$\dot{R} = R\hat{\omega} \tag{2}$$
$$m\dot{v} = -mge_3 + Rf_c + f_d \tag{3}$$
$$J\dot{\omega} = -\omega \times J\omega + \tau_c + \tau_d, \tag{4}$$

where $m \in \mathbb{R}_{>0}$ and $J = J^T \in \mathbb{R}^{3\times3}_{>0}$ are the mass and inertia matrix of the rigid body, respectively. Note that the control wrench (f_c, τ_c) is defined with components in the body frame $\mathcal{F}_B$.

3 Control problem: trajectory tracking in $\mathrm{SO}(3) \times \mathbb{R}^3$ under thrust vectoring constraints

The thrust-vectoring limitation of the actuation mechanism are now formally defined. In the following, the control torque τ_c is assumed to span $\mathbb{R}^3$, *i.e.*, the rotational dynamics is fully actuated. However, the control force f_c spans only the spherical sector, around the third body axis b_3, defined as:

$$0 < \cos(\theta_M) \leq \frac{f_c^T(t)e_3}{\|f_c(t)\|} := \cos(\theta_c(t))$$
$$\|f_c(t)\| \leq f_M \quad \forall t \geq 0. \tag{5}$$

These assumptions may be reasonable approximations for UAVs like the tilt-rotor quadcopter in Figure 1 [5]. Let us now consider a smooth desired trajectory $t \mapsto (R_d(t), x_d(t)) =: G_d(t) \in \mathcal{M}$ that is assigned as a function of time and the corresponding tangent vector that

is given by $t \mapsto \xi_d(t) := (v_d(t), \omega_d(t)) \in T_{G_d}\mathcal{M}$, where $\omega_d(t) = (R_d^T(t)\dot{R}_d(t))^\vee \in \mathbb{R}^3$ is the desired (*body*) angular velocity and $v_d(t) = \dot{x}_d(t) \in \mathbb{R}^3$ is the desired (*inertial*) translational velocity. Due to the thrust vectoring limitation in (5), an arbitrary full-pose trajectory in $\mathcal{M}$ cannot be followed. This can be understood by inspecting the inputs at steady state obtained by inverting the system dynamics:

$$f_c^n(t) := mR_d^T(t)(\dot{v}_d(t) + ge_3) \tag{6}$$
$$\tau_c^n(t) := J\dot{\omega}_d(t) + \omega_d(t) \times J\omega_d(t), \tag{7}$$

in which, for simplicity, we assumed nominal conditions, *i.e.*, $(f_d, \tau_d) = (0, 0)$. Clearly, whereas equation (7) is always fulfilled for any sufficiently smooth trajectory, the control force (6) may not be compatible with constraint (5) for a given desired attitude motion $R_d(t)$ and a given vector $m(\dot{v}_d(t) + ge_3)$. As a consequence, the control objective must be relaxed to deal with the platform underactuation. In particular, since position tracking is of utmost importance in applications involving aerial vehicles, we will devise a strategy that always ensures position tracking and that tries to achieve the attitude tracking objective at best. In this regard, equation (6) provides a useful hint: it is always possible to find a rotation matrix such that the resulting control force is inside the cone region defined by (5). Therefore, it is assumed that the actual attitude reference is at least a twice differentiable curve defined as:

$$t \mapsto R_a(t) \in \mathrm{SO}(3) \cap \mathcal{C}_2, \tag{8}$$

which will be computed dynamically in order to satisfy the cone region constraint (5) and to be as close as possible to the desired attitude $t \mapsto R_d(t)$.

4 Control law design

In this section we propose a control law that ensures uniform global asymptotic tracking (UGAT) for the position dynamics described by equations (1), (3) under the constraint (5). Furthermore, we show that, when the desired full-pose trajectory satisfies a specific trackability condition, the desired attitude motion can be tracked as well from almost-all initial conditions in $T\mathrm{SO}(3)$.

4.1 Position subsystem

First we consider the position dynamics and assume $f_d = 0$ for control design purposes, under the assumption that its contribution is mild in the flight regimes of interest. One can follow the approach in [6] to account for this term; nonetheless, we will verify our solution by taking f_d into account. By assuming the dynamics in (1), (3), the configuration errors for the position and velocity are defined in the inertial frame as

$$e_x := x - x_d, \quad e_v := v - v_d. \tag{9}$$

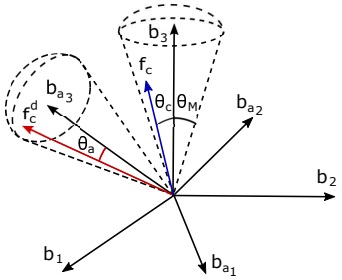

Fig. 2. Spherical sector and control force definition.

By introducing the attitude error $R_e := R_a^T R$, we propose the following control force:

$$f_c := c(R_e)R_a^T f_c^d, \tag{10}$$

where

$$f_c^d := \mathcal{K}(e_x, e_v) + m\left(\dot{v}_d + ge_3\right) \tag{11}$$

and $\mathcal{K}_i(e_x, e_v) := -\sigma_{M_{o_i}}\left(e_{v_i} + k_{x_i}\sigma_{M_{i_i}}\left(e_{x_i} + e_{v_i}\right)\right)$, $i = 1, 2, 3$, is a nested saturation stabilizer, in which $\sigma_M : \mathbb{R} \to \mathbb{R}$ denotes a properly selected twice differentiable version of the standard saturation function and M_{o_i}, $M_{i_i} \in \mathbb{R}_{>0}$ are suitably chosen saturation levels [15]. Notice that f_c^d is the control force, with components defined in the inertial frame, required to track the position trajectory. The function $c : \mathrm{SO}(3) \to \mathbb{R}$ is a scaling factor with the following properties:

$$\lim_{R_e \to I_3} c(R_e) = 1, \quad 0 < c(R_e) \leq c_M, \ \forall R_e \in \mathrm{SO}(3) \tag{12}$$

where c_M is a strictly positive scalar. A possible selection is $c(R_e) := \frac{\ell - (1 - \cos(e_3^T R_e e_3))}{\ell}$ with $\ell > 2$, which satisfies the properties in (12) with $c_M = 1$. With respect to the standard choice $c(R_e) = 1$, our expression scales down the control force when the attitude error is large and therefore reduces the position overshoot (see Section 6.2 for further details about $c(R_e)$). The closed-loop position error dynamics is conveniently written by adding and subtracting the term f_c^d in equation (9) to get:

$$\dot{e}_x = e_v \tag{13}$$
$$m\dot{e}_v = \mathcal{K}(e_x, e_v) + \Delta R(R_e, R_a) f_c^d(e_x, e_v, \dot{v}_d(t)) \tag{14}$$

where $\Delta R(R_e, R_a) := c(R_e)R_a R_e R_a^T - I_3$ weighs the mismatch between the desired control force f_c^d and the one actually delivered in the inertial frame, *i.e.*, Rf_c. Therefore, the position error subsystem is a double integrator perturbed by a term dependent on tracking errors and, in particular, that is vanishing for $R_e \to I_3$.

4.2 Reference attitude computation

This section presents the strategy to compute the reference attitude motion, described by the time evolution of

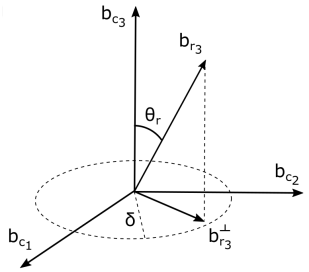

Fig. 3. Third relative axis b_{r_3} and its planar component $b_{r_3}^{\perp}$.

the rotation matrix R_a, to deal with the platform underactuation. Building on the ideas developed in Section 3, we will exploit the fact that it is always possible to find a set of attitude configurations R_a that makes f_c compatible with constraint (5). As this set is not a singleton, one can try to select a reference attitude as close as possible to the desired one. Differently from the static planning of [5], our strategy is based on a dynamic computation of the reference attitude motion that tracks $t \mapsto R_d(t)$ as long as the control force satisfies constraint (5). Therefore, R_a will depend both on terms related to position errors and on terms related to the desired trajectory. A convenient choice is to decompose the reference rotation matrix R_a by exploiting the group operation in SO (3) as follows:

$$R_a := R_c R_r \tag{15}$$

where R_r is a relative rotation matrix, whose role will be addressed in the next section (4.2.1), and R_c is a rotation matrix defined following standard strategies. For instance, a possible selection is [10]:

$$R_c := \left[\, b_{c_1} \;\; b_{c_2} \;\; b_{c_3} \,\right]$$
$$b_{c_3} := \frac{f_c^d}{\|f_c^d\|},\; b_{c_2} := \frac{b_{c_3} \times b_d}{\|b_{c_3} \times b_d\|},\; b_{c_1} := b_{c_2} \times b_{c_3}, \tag{16}$$

in which $b_d(t) = \left[\, \cos(\psi_d(t)) \;\; \sin(\psi_d(t)) \;\; 0 \,\right]^T$ and $\psi_d(t)$ is the desired yaw angle (which may be extracted from $R_d(t)$). The definition of the base orientation (16) becomes indeterminate in the degenerate cases when $\|f_c^d\| = 0$ and b_{c_3} is parallel to b_d [10]. Next, we propose a solution such that these conditions can be avoided altogether. Let us assume that the lower bound on the third component of f_c^d in (11) is greater than zero, *i.e.*, $f_{m_3}^d := m \inf_{t \geq 0} |\dot{v}_{d_3}(t) + g| > 0$. Then, by inspecting the expression of f_c^d, if one selects $\mathcal{K}_{M_3} = M_{o_3} < f_{m_3}^d$, it is easily proved that $\|f_c^d(t)\| \geq |f_{c_3}^d(t)| \geq f_{m_3}^d - \mathcal{K}_{M_3} > 0$. Note that $\|b_{c_3} \times b_d\|$ does not vanish either, because $b_d(t)$ belongs the horizontal plane (e_1, e_2) and the third component of $b_{c_3}(t)$ is different from zero $\forall t \geq 0$.

4.2.1 Relative attitude

The idea behind the decomposition of the reference attitude in (15) is that $R_r \in \mathrm{SO}(3)$ can be exploited as an additional degree of freedom to try to track the desired attitude motion $t \mapsto R_d(t)$ while satisfying constraint (5). We address these issues separately, by first considering the thrust vectoring constraint. As $R_r \in \mathrm{SO}(3)$, it can be generated, dynamically, by applying an input $\hat{\omega}_r \in \mathfrak{so}(3)$ as follows:

$$\dot{R}_r = \hat{\omega}_r R_r. \tag{17}$$

Notice that the rotation matrix $R_r := [b_{r_1}\, b_{r_2}\, b_{r_3}]$ has components with respect to the frame $\mathcal{F}_c$ defined by (16).

Cone region constraint handling

The following proposition confirms that by properly computing $R_a(t)$, the control force will be kept inside the cone defined by the spherical sector constraint (5).

Proposition 1 *Consider the unit vectors $b_{c_3} := R_c e_3$ (16) and $b_{a_3} := R_a e_3$. If $\cos(\theta_a) := b_{c_3}^T b_{a_3}$ is kept larger than $\cos(\theta_M) > 0$ $\forall t \geq 0$ then, the spherical sector constraint in equation (5) is satisfied.*

PROOF. By substituting the definition of the control force (10) in equation (5), we get:

$$\cos(\theta_c) = \frac{e_3^T f_c}{\|f_c\|} = \frac{c(R_e) e_3^T R_a^T f_c^d}{\|c(R_e) R_a^T f_c^d\|} = b_{a_3}^T b_{c_3} = \cos(\theta_a). \tag{18}$$

Thanks to this equivalence, the spherical sector constraint is satisfied as long as $\cos(\theta_a) \geq \cos(\theta_M)$ (See Figure 2 for a visual interpretation).

Furthermore, with the decomposition (15) in place, constraint (5) can be satisfied by keeping the cosine of the relative angle θ_r (Figure 3) greater than $\cos(\theta_M)$. Indeed, considering Proposition 1, we have $\cos(\theta_c) = \cos(\theta_a)$, and the following equality holds $\forall t \geq 0$:

$$\cos(\theta_a) = b_{c_3}^T R_a e_3 = b_{c_3}^T R_c R_r e_3 = e_3^T b_{r_3} =: \cos(\theta_r). \tag{19}$$

To keep $\cos(\theta_r) \geq \cos(\theta_M)$, we propose the following expression for the angular velocity input ω_r:

$$\omega_r := b_{r_3} \times \mathrm{Proj}_G(b_{r_3}, \bar{\omega}_r \times b_{r_3}) + (\bar{\omega}_r^T b_{r_3}) b_{r_3}, \tag{20}$$

where $\bar{\omega}_r \in \mathbb{R}^3$ and $\mathrm{Proj}_G : \mathbb{S}^2 \times \mathbb{R}^3 \to \mathbb{R}^3$ is a sufficiently smooth projection operator that removes the radial component of the angular velocity in the plane defined by b_{c_1}, b_{c_2}, so that the axis b_{r_3} will never leave the cone associated to the spherical sector (5) (while keeping $b_{r_3} \in \mathbb{S}^2$, see Appendix A.1 for details). Basically, the planar components of $b_{r_3}^{\perp} := \left[\, {}^{b_{r_3}}{}_{1} \;\; {}^{b_{r_3}}{}_{2} \,\right]^T$ are kept within a circle of radius $\delta := \sin(\theta_M)$. According to equation (20), the

component of $\bar{\omega}_r$ along b_{r_3} is preserved, whereas the planar component of $\dot{b}_{r_3}$, *i.e.*, $\dot{b}_{r_3}^{\perp} := ((I_3 - b_{r_3} b_{r_3}^T)\bar{\omega}_r)^{\perp}$ is modified only when b_{r_3} is trying to leave the cone associated to (5). The projection operator starts working when

$$\|b_{r_3}^{\perp}\| \in \left(\tfrac{\delta}{\sqrt{1+\varepsilon}}, \delta\right] \wedge (\dot{b}_{r_3}^{\perp})^T b_{r_3}^{\perp} > 0, \tag{21}$$

where $\varepsilon \in (0,1)$ is a design parameter, enabling a smooth transition towards the bound δ. Hence, the b_{r_3} axis is kept inside the cone defined by the angle θ_M around b_{c_3} and, by referring to (19), it is possible to infer that

$$\cos(\theta_c(t)) = \cos(\theta_r(t)) \geq \cos(\theta_M) \quad \forall t \geq 0. \tag{22}$$

As a consequence, if b_{r_3} is inside the cone described by (5) at initial time, it will never leave it: for instance, it is enough to choose $R_r(0) = I_3$.

Desired attitude tracking

By applying a generic input $t \mapsto \bar{\omega}_r(t) \in \mathbb{R}^3 \cap \mathcal{C}^1$ through equation (20), we obtain a reference attitude motion $R_a(t)$ whose third axis never gets out from a cone around b_{c_3} with an angle θ_M, thus satisfying equation (5). However, $R_a(t)$ will be different from $R_d(t)$. Clearly, if $\cos(\theta_d(t)) \geq \cos(\theta_M)$, where $\cos(\theta_d) := \frac{e_3^T f_c^n}{\|f_c^n\|}$ with f_c^n defined in equation (6), then, the desired attitude is trackable and we would like the reference attitude R_a to converge to R_d. To tackle this problem, $\bar{\omega}_r$ can be used as an intermediate control variable of a tracking problem on $\mathrm{SO}(3)$, in which we define the reference attitude error as $\bar{R}_e := R_a R_d^T$. By selecting

$$\bar{\omega}_r := R_r \omega_d - \omega_c - R_r R_d^T \bar{e}_R, \tag{23}$$

where $\bar{e}_R$ is the left-trivialized derivative of a polar Morse function $\Psi_a(\bar{R}_e)$, the reference attitude R_a follows the desired attitude R_d, whenever this is feasible. Finally, the modified attitude reference and its time derivatives, which are required to compute the control torque as shown in Section 4.3, are given by:

$$\dot{R}_a = R_a \hat{\omega}_a \tag{24}$$
$$\omega_a = R_r^T (\omega_c + \omega_r) \tag{25}$$
$$\dot{\omega}_a = -R_r^T \hat{\omega}_r \omega_c + R_r^T (\dot{\omega}_c + \dot{\omega}_r) \tag{26}$$

where ω_c and $\dot{\omega}_c$ are the the angular velocity and acceleration of the frame $\mathcal{F}_C := (O_B, \{b_{c_1}, b_{c_2}, b_{c_3}\})$. They can be obtained by taking the first and second time derivatives of $R_c(t)$:

$$\omega_c := (R_c^T \dot{R}_c)^{\vee}, \quad \dot{\omega}_c := (R_c^T \ddot{R}_c - \hat{\omega}_c^2)^{\vee}, \tag{27}$$

which is possible when assuming $t \mapsto x_d(t) \in \mathbb{R}^3 \cap \mathcal{C}^4$ and $t \mapsto R_d(t) \in \mathrm{SO}(3) \cap \mathcal{C}^2$.
Before going on, the following result is instrumental in proving that the desired attitude can be tracked under a specific condition.

Proposition 2 *Consider equations* (17), (20) *for a given relative angular velocity* $t \mapsto \bar{\omega}_r(t) \in \mathbb{R}^3$ *and a smooth geometric*[1] *projection operator* $\mathrm{Proj}_G : \mathbb{S}^2 \times \mathbb{R}^3 \to \mathbb{R}^3$ *with the properties in* (21). *When* $\|b_{r_3}^{\perp}\| \leq \frac{\delta}{\sqrt{1+\varepsilon}}$ *or when* $(\dot{b}_{r_3}^{\perp})^T b_{r_3}^{\perp} \leq 0$, *it holds that* $\omega_r = \bar{\omega}_r$.

PROOF. According to (21), $\mathrm{Proj}_G(b_{r_3}, \bar{\omega}_r \times b_{r_3}) = \bar{\omega}_r \times b_{r_3}$ whenever $b_{r_3}^{\perp}$ is strictly inside the circle with radius $\frac{\delta}{\sqrt{1+\varepsilon}}$ or $(\dot{b}_{r_3}^{\perp})^T b_{r_3}^{\perp} \leq 0$ where $\dot{b}_{r_3}^{\perp} := ((I_3 - b_{r_3} b_{r_3}^T)\bar{\omega}_r)^{\perp}$. In this condition, this implies that equation (20) reads:

$$\begin{aligned} \omega_r &= b_{r_3} \times \mathrm{Proj}_G(b_{r_3}, \bar{\omega}_r \times b_{r_3}) + (\bar{\omega}_r^T b_{r_3}) b_{r_3} \\ &= b_{r_3} \times (\bar{\omega}_r \times b_{r_3}) + (\bar{\omega}_r^T b_{r_3}) b_{r_3} := \bar{\omega}_r. \end{aligned} \tag{28}$$

4.3 Attitude subsystem

The objective of the control torque is to track the modified reference $R_a(t)$. By referring to the attitude errors

$$R_e := R_a^T R, \quad e_\omega := \omega - R_e^T \omega_a, \tag{29}$$

we can employ the geometric PID law proposed in [11]:

$$\tau_c := -k_R e_R - k_\omega e_\omega - k_I \omega_I + \tau_f(R_e, e_\omega, \omega_d) \tag{30}$$
$$\dot{\omega}_I := -\tfrac{1}{2}(\hat{e}_\omega \omega_I - J^{-1}(\widehat{J\omega_I} e_\omega + \widehat{Je_\omega}\omega_I)) + J^{-1} e_R,$$

where e_R is the left-trivialized derivative of a polar Morse function Ψ_R (see the Notations section) whilst τ_f is a feedforward torque to obtain an autonomous closed-loop (see [11] for more details).

5 Main result

In this section we present the main contribution of this work. With respect to [6], we provide an explicit trackability condition for the desired trajectory. Then, under this condition, we prove that the proposed control law guarantees AGAT while accounting for the spherical sector constraint (5). When the trackability condition is not satisfied, only UGAT for the position subsystem is achieved while the attitude $R(t)$ converges uniformly to $R_a(t)$ from almost all initial conditions in $T\mathrm{SO}(3)$. The proof hinges on the analysis of the cascaded connection between the attitude and position error subsystems, which is realized through the term $\Delta R f_c^d$ in equation(14).

[1] See Appendix A.1 for the definition of the geometric projection operator

Theorem 3 *Consider the system described by equations* (1)-(4)*, subjected to constraint* (5)*, with the control laws* (10), (30)*, assume a constant disturbance torque* $\tau_d \in \mathcal{L}_\infty$*,* $f_d = 0$ *and a reference attitude motion defined by* (24), (25) *complemented with* (20), (23)*. Given a desired attitude motion* $t \mapsto R_d(t) \in SO(3) \cap \mathcal{C}^2$ *and a position trajectory* $t \mapsto x_d(t) \in \mathbb{R}^3 \cap \mathcal{C}^4$ *with a bounded acceleration profile* $\dot{v}_d(\cdot) \in \mathcal{L}_\infty$ *such that* $\sup_{t\geq 0} \|m(\dot{v}_d(t) + ge_3)\| < f_M$ *and* $m \inf_{t\geq 0} |\dot{v}_{d_3}(t) - g| > 0$*, if there exists* $\bar{t} \geq 0$ *for which*

$$\frac{e_3^T f_c^n(t)}{\|f_c^n(t)\|} \geq \cos(\bar{\theta}_M) \; \forall t \geq \bar{t} \geq 0, \tag{31}$$

where f_c^n *is defined in equation* (6)*,* $\bar{\theta}_M := \arcsin\left(\frac{\delta}{\sqrt{1+\epsilon}}\right)$*,* $\delta := \sin(\theta_M)$ *and* $\varepsilon \in (0,1)$ *is a design parameter, then, there exist control gains* k_{x_i}, k_R*,* k_ω*,* k_I *and saturation levels* M_{o_i}*,* M_{i_i} $(i = 1,2,3)$ *such that the trajectory* $t \mapsto (R_e(t), e_\omega(t), e_x(t), e_v(t), R_a(t))$ *converges to* $(I_3, 0, 0, 0, R_d(t))$ *with basin of attraction containing almost-all* $(R_e, e_\omega) \in T\mathrm{SO}(3)$*,* $(e_x, e_v) \in \mathbb{R}^3 \times \mathbb{R}^3$ *and* $R_a \in \{R \in \mathrm{SO}(3) : e_3^T R^T R_c(0) e_3 \geq \cos(\theta_M)\}$*.*

PROOF. The proof is based on the small signal ISS property of the nested saturation stabilizer used in equation (11) and on the selection of the scaling factor $c(R_e)$ satisfying (12). Combining the equations of motion and the control laws with the definition of the errors, the closed-loop dynamics is a cascade interconnection in which the (autonomous) attitude error subsystem perturbs the position error dynamics through the interconnection term $\Delta R f_c^d$. Then, the output of the position error subsystem is used to generate the reference attitude $R_a(t)$ according to equations (24)-(25) and (20), (23), which is evolving on the compact manifold SO(3) and it is well defined by selecting $M_{o_3} < m \inf_{t\geq 0} |\dot{v}_{d_3}(t) + g|$ (see the reasoning below equation (16)). By applying the control torque in equation (30) to the attitude dynamics (2),(4), the equilibrium point $(R_e, e_\omega) = (I_3, 0)$ is AGAS for any sufficiently smooth reference, as the one computed according to (24), (25) and (20),(23), following the results in [11]. It can be shown, taking similar steps as in the proof of [7, Prop. 4], that the interconnection term is bounded as $\|\Delta R(R_e, R_a) f_c^d\| \leq \gamma(\Psi_{k_R I_3}(R_e)) f_{c_M}^d$ where $\gamma(\cdot)$ is a class-$\mathcal{K}_\infty$ function and $f_{c_M}^d := \sqrt{3}\sum_{i=1}^3 M_{o_i} + \sup_{t\geq 0} \|m(\dot{v}_d + ge_3)\|$. By considering (10) and (12), we get $\|f_c\| = |c(R_e)| \|R_a^T f_c^d\| \leq c_M f_{c_M}^d$ and the bound on the control force magnitude in (5) is satisfied by selecting $\sqrt{3}\sum_{i=1}^3 M_{o_i} \leq f_M - \sup_{t\geq 0} \|m(\dot{v}_d(t) + ge_3)\|$, which is possible thanks to the assumption that $f_M > \sup_{t\geq 0} \|m(\dot{v}_d(t) + ge_3)\|$. By considering Proposition 1, $e_3^T R_a^T(0) R_c(0) e_3 = \cos(\theta_a(0)) = \cos(\theta_c(0)) \geq \cos(\theta_M)$, and the constraint (5) is satisfied at $t = 0$. Thanks to the properties of the projection operator in equation (22), $\cos(\theta_c(t)) \geq \cos(\theta_M) \; \forall t \geq 0$ and constraint (5) is satisfied. Then, we can invoke arguments similar to the proof of [12, Prop. 4] or [15, Thm. 7.4] to conclude the stability of the cascade and the UGAS of the zero equilibrium of the position error dynamics. We can prove that, under the trackability condition (31), $R_a(t) \to R_d(t)$, by showing that there is a time instant starting from which the time derivative of the Lyapunov function $\Psi_a(\bar{R}_e)$, from which $\bar{e}_R$ in equation (23) is computed, is strictly negative definite along the trajectories of the system. By direct computation, one gets:

$$\begin{aligned} \dot{\Psi}_a(\bar{R}_e) &= \left(R_d^T \bar{e}_R\right)^T (\omega_a - \omega_d) \\ &= \left(R_d^T \bar{e}_R\right)^T \left(R_r^T (\omega_c + \omega_r) - \omega_d\right). \end{aligned} \tag{32}$$

When considering equation (31) and the uniform convergence of the tracking error $(R_e, e_\omega, e_x, e_v)$ to $(I_3, 0, 0, 0)$, there will be a time $\tilde{t} \geq 0$ starting from which the projection operator is not working, namely $\mathrm{Proj}_G(b_{r_3}, \bar{\omega}_r \times b_{r_3}) = \bar{\omega}_r \times b_{r_3}$, because at least one of the conditions in (21) is satisfied. In this case, through Proposition 2, $\omega_r = \bar{\omega}_r$ and, by substituting the definition (23) of $\bar{\omega}_r$ in equation (32), $\dot{\Psi}_a(\bar{R}_e) = -\|\bar{e}_R\|^2 \; \forall t \geq \tilde{t}$ and $R_a(t) \to R_d(t)$.

6 Numerical results

In this section two simulation examples are presented to demonstrate the effectiveness of the proposed controller, when applied to a tilt-rotor quadcopter UAV.
This platform (Figure 1) is an aerial vehicle equipped with four propellers that can be tilted independently. It has an over-actuated configuration with eight control inputs (four angular velocities ω_{r_i} and four angles α_i, $i = 1,2,3,4$) that can be exploited to apply the required control wrench (f_c, τ_c) according to equation (10) and (30). In particular, the mixer map that relates the actual inputs and the control wrench is invertible as shown in [7]. The simulation model is a multi-body system with nine rigid bodies, developed in the Modelica modeling language, augmented to include the dynamics of the tilting servo-actuators (third-order models) and of the motor/propeller groups (first-order models) to increase the reliability of the simulation. Furthermore, body-drag and induced-drag forces are accounted for as well as the aerodynamic damping torque, following [2]. Specifically, we consider $\tau_d := D_a \omega$, where $D_a = -\mathrm{diag}(0.046, 0.046, 0.019)$, and a simplified model of the disturbance force, *i.e.*, $f_d := -c_d \|v\| v - \sum_{i=1}^4 c_I \sqrt{T_i}(v_i - (v_i^T u_i) u_i)$, in which $c_d = 0.01$, $c_I = 0.1$ are the body and induced drag coefficients, respectively, v_i is the velocity of the hub of the *i-th* rotor, u_i is the unit vector describing the current orientation of the *i-th* propeller axis and T_i is the thrust delivered by the *i-th* rotor. A constant torque disturbance $\tau_d = \begin{bmatrix} 0.03 & 0.03 & 0.03 \end{bmatrix}^T$ Nm is also included to model the effect of unbalanced rotors.

For the sake of conciseness, only the nominal inertial values used for control tuning are reported: the UAV inertia matrix is $J = \mathrm{diag}\,(0.0074,\, 0.0074,\, 0.05)\,\mathrm{kgm}^2$ while its mass is $m = 1.9\mathrm{kg}$. The maximum tilt-angle θ_M is set to 30°, which defines the admissible cone region according to (5). The selected controller gains are $k_R = 1.7$, $k_\omega = 0.5\,k_I = 0.01$, $k_x = \{10, 10, 10\}$, $\ell = 2.1$ and $\Psi_a := \Psi_{2k_R I_3}(\bar{R}_e)$, $\Psi_R := \Psi_{I_3}(R_e)$. The parameter of the projection operator is set to $\varepsilon = 0.05$ and the saturation levels to $L_{i_i} = 4.5\mathrm{N}, L_{o_i} = 17\mathrm{N}$, $M_{i_i} = 5\mathrm{N}$, $M_{o_i} = 18\mathrm{N}$, for $i = 1, 2, 3$, according to the definition of the saturation function in [15, Pag. 129]. In this way, we ensure that the control force is bounded and its magnitude never vanishes.

6.1 *Eight-shaped trajectory tracking*

We consider an eight-shaped trajectory, $x_d(t) := \left[\begin{array}{ccc} \frac{\sin(2\omega_p t)}{3-\cos(2\omega_p t)} & \frac{2\cos(\omega_p t)}{3-\cos(2\omega_p t)} & 1 \end{array}\right]^T \mathrm{m}$, $\omega_p = \frac{2\pi}{8}\mathrm{rads}^{-1}$, and a rotational maneuver $R_d(t) := \left[\begin{array}{ccc} t_d(t) & n_d(t) & b_d \end{array}\right] \exp(\theta_d(t)\hat{e}_1)$ where $t_d(t) = \frac{v_d(t)}{\|v_d(t)\|}$ is the tangent vector to the curve $x_d(t)$, $b_d = \left[\begin{array}{ccc} 0 & 0 & 1 \end{array}\right]^T$ and $n_d(t) = t_d(t) \times b_d$. The desired attitude corresponds to a roll motion around the axis t_d, with the profile $\theta_d(t)$ made of two constant segments of 25° and 15°, connected by smooth curves, as shown in Figure 5. Notice that the required attitude motion is close to the angle $\theta_M = 30°$ which defines the cone region in (5). The desired trajectory (dotted line) is shown in the small box in Figure 4, together with the actual path followed by the UAV (solid line) for three complete rounds, starting from a misplaced hovering condition at $x(0) = \left[\begin{array}{ccc} 1.1 & 0 & 1 \end{array}\right]^T \mathrm{m}$. Figure 4 confirms that the position error is bounded. The attitude tracking performance is illustrated in Figure 5, where the inclination angle of the vehicle $\theta_v := \arccos(b_3^T e_3)$ and the desired angle $\theta_d(t)$ are shown together with the angle $\theta_c(t)$ between the control force f_c and the third-body axis b_3. It is clear that even in the presence of unmodeled dynamics, the spherical sector constraint (5) is satisfied. In particular, the projection operator starts working during the most demanding phase of the attitude maneuver when the desired attitude is not tracked exactly in order to guarantee position tracking: as expected, the position tracking performance is not deteriorated. Note that from Theorem 3, when the desired attitude is trackable, the desired attitude is tracked exactly (up to the effects of unmodeled disturbances).

6.2 *Large attitude error recovery*

We consider now the case of an attitude recovery maneuver in order to show the benefit that can be gained by exploiting the scaling factor $c(R_e)$ introduced in the control force (10). When the attitude error is large, the control force f_c delivered according to (10) is directed along a direction that is pushing the UAV away from the desired trajectory (to account for (5)) and, with the selection $c(R_e) = 1$, it may have a large magnitude to compensate for gravity, desired acceleration and position errors. Indeed, to handle the platform underactuation, the control force f_c is necessarily delivered inside the spherical sector and cannot instantaneously be set equal to the desired control force f_c^d defined in (11). Therefore, in this condition, it is convenient to scale the magnitude of f_c while waiting for the attitude error decrease. To highlight this, we consider the case of a quadcopter being dropped with the reference plane perpendicular to the ground: $x(0) = \left[\begin{array}{ccc} 0 & 0 & 1 \end{array}\right]^T \mathrm{m}$, $v(0) = \left[\begin{array}{ccc} 0.5 & 0 & 0 \end{array}\right]^T \mathrm{ms}^{-1}$ and $R(0) = \exp\left(\frac{\pi}{2}\hat{e}_2\right)$, $\omega(0) = \left[\begin{array}{ccc} 0 & 0 & 0 \end{array}\right]^T \mathrm{rads}^{-1}$. The set-point is the hovering condition at $x(0) = \left[\begin{array}{ccc} 0 & 0 & 1 \end{array}\right]^T \mathrm{m}$. At the initial time, the desired force $f_c^d(0)$ is almost directed along e_3; however, due to constraint (5), the control force (10) is delivered inside a cone around b_3, which is aligned with e_2 at the initial time. Clearly, in this condition, the inevitable position overshoot depends on $\|f_c\| = c(R_e)\|f_c^d\|$. In this simulation we compare the performance of our solution, *i.e.*, $c(R_e) := \frac{\ell - (1-\cos(e_3^T R_e e_3))}{\ell}$, with the standard choice $c(R_e) = 1$ [6,12]. It is worth remarking that the approach in [10] cannot be tested since it would result in $\|f_c\| = 0\,\mathrm{N}$. Note that at the initial time our approach provides $c(R_e(0)) \approx 0.5$. With respect to the previous simulation, $k_x = \{15, 15, 15\}$ and $k_I = 0.05$. Figure 6 shows that the percentage difference of overshoot in the position tracking is reduced of about 20%.

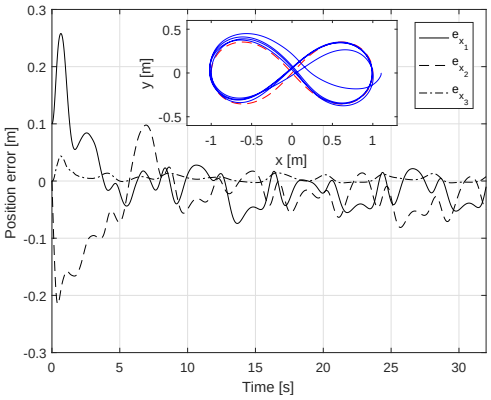

Fig. 4. (A) Position tracking error - e_x.

7 Conclusions

In this paper, the problem of designing a control law for UAVs with thrust vectoring capabilities has been addressed. Geometric control theory has been exploited to develop a control law which guarantees AGAT on $\mathrm{SO}(3) \times \mathbb{R}^3$ when the desired motion is trackable, even in the presence of actuation constraints. Specifically, the total control force is kept within a spherical sector defined by the maximum tilt-angle and deliverable thrust

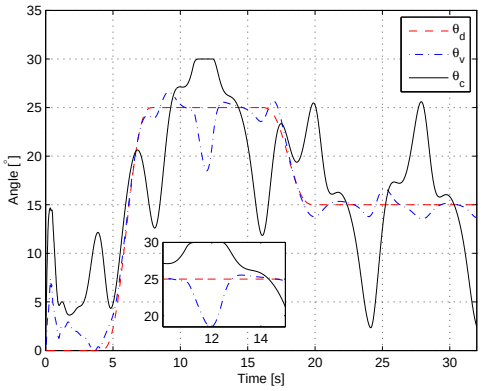

Fig. 5. (A) Attitude tracking and cone region validation.

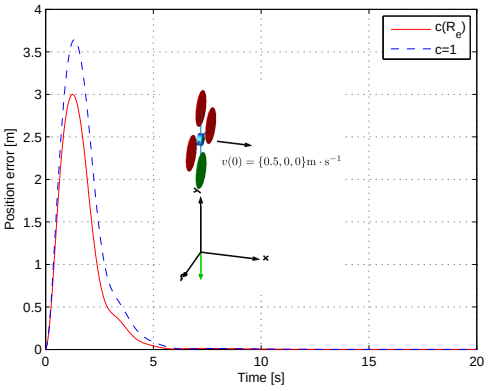

Fig. 6. (B) Position errors comparison - $\|e_x\|$.

of the propulsive system. This is obtained by relaxing the attitude tracking objective: a reference attitude is computed as the output of a controller that tries to track the desired attitude motion while keeping into account the thrust vectoring limitation. Numerical simulations have been performed to test the control law.

References

[1] A. Abdessameud and A. Tayebi. Global trajectory tracking control of VTOL-UAVs without linear velocity measurements. *Automatica*, 46(6):1053–1059, 2010.

[2] M. Bangura. *Aerodynamics and Control of Quadrotors*. PhD thesis, College of Engineering and Computer Science, The Australian National University, 2017.

[3] Z. Cai, M. S. de Queiroz, and D. M. Dawson. A sufficiently smooth projection operator. *IEEE Transactions on Automatic Control*, 51(1):135–139, Jan 2006.

[4] B. Crowther, A. Lanzon, M. Maya-Gonzalez, and D. Langkamp. Kinematic analysis and control design for a nonplanar multirotor vehicle. *Journal of Guidance, Control, and Dynamics*, 34(4):1157–1171, 2011.

[5] A. Franchi, R. Carli, D. Bicego, and M. Ryll. Full-pose tracking control for aerial robotic systems with laterally bounded input force. *IEEE Transactions on Robotics*, PP(99):1–8, 2018.

[6] M.D. Hua, T. Hamel, P. Morin, and C. Samson. Control of VTOL vehicles with thrust-tilting augmentation. *Automatica*, 52(2):1–7, feb 2015.

[7] D. Invernizzi and M. Lovera. Geometric tracking control of a quadcopter tiltrotor UAV. In *20th IFAC World Congress, Toulouse, France*, 2017.

[8] G. Jiang and R. Voyles. A nonparallel hexrotor UAV with faster response to disturbances for precision position keeping. In *2014 IEEE International Symposium on Safety, Security, and Rescue Robotics*, pages 1–5. IEEE, 2014.

[9] D. E. Koditschek. The Application of Total Energy as a Lyapunov Function for Mechanical Control Systems. *J. E. Marsden, P. S. Krishnaprasad and J. C. Simo (Eds) Dynamics and Control of Multi Body Systems*, 97:131–157, February 1989.

[10] T. Lee, M. Leok, and H. McClamroch. Geometric tracking control of a quadrotor UAV on SE(3). In *IEEE Conference on Decision and Control, Atlanta, USA*, 2010.

[11] D. H. S. Maithripala and J. M. Berg. An intrinsic PID controller for mechanical systems on Lie groups. *Automatica*, 54(4):189–200, 2015.

[12] R. Naldi, M. Furci, R. G. Sanfelice, and L. Marconi. Robust global trajectory tracking for underactuated VTOL aerial vehicles using inner-outer loop control paradigms. *IEEE Transactions on Automatic Control*, 62(1):97–112, 2017.

[13] J. M. Pflimlin, P. Souères, and T. Hamel. Position control of a ducted fan vtol uav in crosswind. *International Journal of Control*, 80(5):666–683, 2007.

[14] S. Rajappa, M. Ryll, H. H. Bülthoff, and A. Franchi. Modeling, control and design optimization for a fully-actuated hexarotor aerial vehicle with tilted propellers. In *2015 IEEE International Conference on Robotics and Automation*, pages 4006–4013. IEEE, 2015.

[15] I. A. Raptis and K. P. Valavanis. *Linear and Nonlinear Control of Small-Scale Unmanned Helicopters*. Springer Netherlands, 2010.

[16] A. Roberts and A. Tayebi. Adaptive position tracking of VTOL UAVs. *IEEE Transactions on Robotics*, 27(1):129–142, 2011.

[17] M. Ryll, H. H. Bülthoff, and P. Robuffo Giordano. A novel overactuated quadrotor unmanned aerial vehicle: Modeling, control, and experimental validation. *IEEE Transactions on Control Systems Technology*, 23(2):540–556, March 2015.

A Appendix

A.1 Geometric projection operator

To keep $t \mapsto b_{r_3}(t)$ in $\mathbb{S}^2$, it is possible to define $\text{Proj}_G : \mathbb{S}^2 \times \mathbb{R}^3 \to \mathbb{R}^3$ as follows: the projection operator $\text{Proj}(y, \dot{y}) : \mathbb{R}^n \times \mathbb{R}^n \to \mathbb{R}^n$ proposed in [3] is used for the planar components of b_{r_3}, *i.e.*, $\dot{b}_{r_3}^{\perp} := \text{Proj}_G^{\perp}(b_{r_3}, \bar{\omega}_r \times b_{r_3}) := \text{Proj}(b_{r_3}^{\perp}, (\bar{\omega}_r \times b_{r_3})^{\perp})$, then, the dynamics of the out-of-plane component is assigned as $\dot{b}_{r_{3_3}} := \text{Proj}_{G_3}(b_{r_3}, \bar{\omega}_r \times b_{r_3}) := -\frac{b_{r_{3_1}} \dot{b}_{r_{3_1}} + b_{r_{3_2}} \dot{b}_{r_{3_2}}}{\sqrt{1 - b_{r_{3_1}}^2 - b_{r_{3_2}}^2}}$.